Energy recovery linac (ERL) coherent hard x-ray sources

2010 New J. Phys. 12 035011

(http://iopscience.iop.org/1367-2630/12/3/035011)

New Journal of Physics
The open-access journal for physics

Energy recovery linac (ERL) coherent hard x-ray sources

Donald H Bilderback[1,2], Joel D Brock[1,2], Darren S Dale[1], Kenneth D Finkelstein[1], Mark A Pfeifer[1] and Sol M Gruner[1,3]

[1] Cornell High Energy Synchrotron Source, Cornell University, Ithaca, NY 14853, USA
[2] School of Applied and Engineering Physics, Cornell University, Ithaca, NY 14853, USA
[3] Department of Physics, Cornell University, Ithaca, NY 14853, USA
E-mail: smg26@cornell.edu

New Journal of Physics **12** (2010) 035011 (27pp)
Received 24 November 2009
Published 31 March 2010
Online at http://www.njp.org/
doi:10.1088/1367-2630/12/3/035011

Abstract. Energy recovery linacs (ERLs) have the potential to be superb coherent hard x-ray sources. ERLs are described with reference to a 5 GeV ERL design being studied at Cornell University. The properties of this ERL, and the x-ray beams that may be produced, are described and spectral curves are calculated and compared to other existing and future x-ray sources. It is shown that ERL and x-ray free electron laser (X-FEL) sources are complementary in terms of the experiments they may optimally serve. ERLs will be especially advantageous in a variety of coherent and nanobeam experiments where the sample must be repetitively probed and in cases where the samples are unique and the requisite scattering information cannot be obtained with a single X-FEL pulse. ERL strengths are elaborated relating to the very high coherent flux, inherently round beams, flexibility and quasi-continuous time structure of the sources. Examples are given where these x-ray characteristics will facilitate advancement of important 'big challenge' areas of science.

Contents

1. Introduction

1.1. What is an energy recovery linac (ERL) x-ray source?

For nearly a century, x-rays have been the primary probe used to determine the atomic structure of matter. For most of this time, the intensity and brilliance of conventional metal-target x-ray sources limited studies to the time-independent examination of macroscopic specimens. The types of x-ray studies that are feasible increased dramatically when synchrotron radiation (SR) x-ray storage ring sources started to become available in the 1970s. Today, almost all operating hard x-ray SR facilities are based on storage ring sources. The accelerator physics of storage rings is well understood and is constrained by the requirement that the electron bunches be able to circulate for hours with minimal losses. In general, it is desirable to maximize the flux and spectral brightness of the x-ray beams, while minimizing the source transverse size and the temporal length of the x-ray pulses. These characteristics follow directly from the bunch transverse and longitudinal emittances and the current circulating in the storage ring. The circulating electrons are subject to perturbations arising from the magnetic forces of the lattice that comprises the storage ring, SR emission, electron–electron interactions and periodic acceleration through radio-frequency (RF) cavities, with resulting equilibrium emittances characteristic of the lattice. Significantly, this equilibrium sets in relatively slowly, typically over milliseconds, corresponding to thousands of turns of a given bunch around the

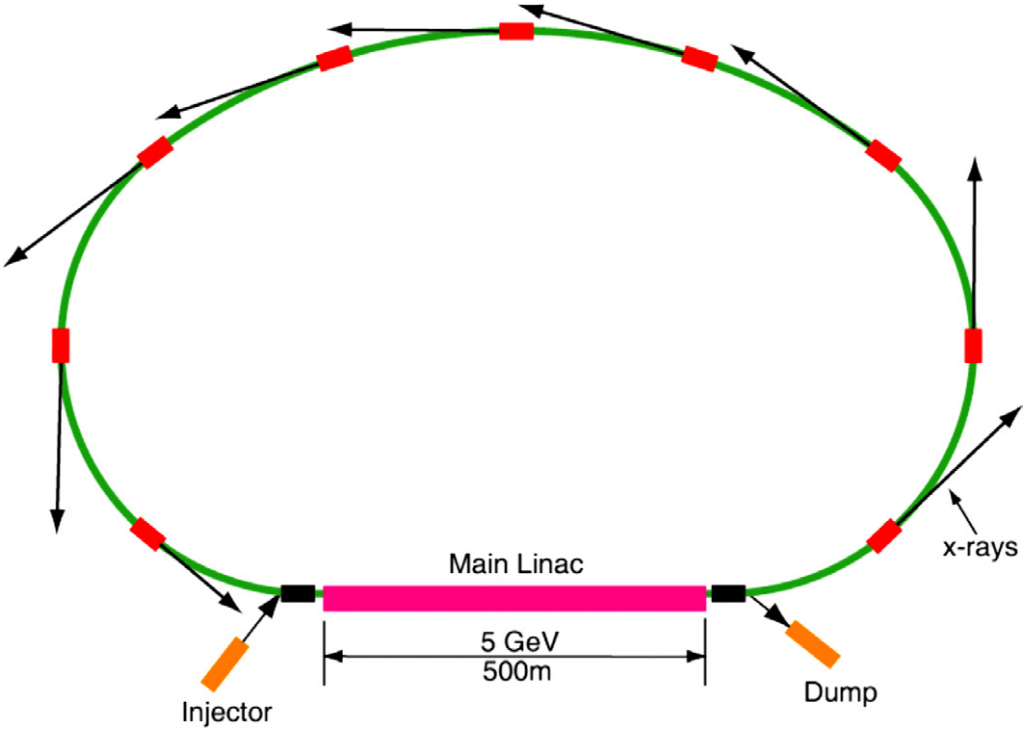

Figure 1. A schematic design of an x-ray ERL. See the text for an explanation. The green transport loop contains undulators (red) to provide beams simultaneously to many x-ray beamlines.

ring. While storage ring technology continues to improve and further advances may be expected, the consensus in the accelerator physics community is that the technology is mature and at the point of diminishing returns [1]–[3].

Although it is possible to use laser-driven photocathodes to produce bunches that initially have superior bunch dimensions and emittances, these bunches cannot be stored without degradation as the storage ring equilibrium sets in. However, bunches can be accelerated in linacs without emittance degradation. This suggests an alternative approach wherein a high duty factor photoinjector is used to feed a linac to produce high-energy bunches. These are passed through undulators to produce highly brilliant SR. The difficulty with this scheme is that a high flux of hard x-rays requires both a reasonably high current and high energy, resulting in an enormous beam power (e.g. 100 mA at 5 GeV is a beam power of 500 MW). It is impractical to produce such beams continuously unless the beam energy is somehow recovered or stored.

A way around this dilemma follows from the observation that linacs can also serve as decelerators by converting electron beam power to RF power in the linac cavity. Tigner [4] noted that the Q of superconducting RF cavities can, in principle, be sufficiently high that this recovered energy may be stored in the cavity long enough to accelerate new particles.

This leads to the ERL concept shown in figure 1. In an ERL source, an injector produces very low emittance bunches, which are then accelerated to high energy in a superconducting linac. These high-energy bunches are passed into a transport loop, similar to a section of a third-generation storage ring, which includes undulators for the production of x-rays. As opposed to the situation in a storage ring, where the equilibrium emittance is achieved during thousands of

passes around the ring, in the ERL the bunch properties are not appreciably degraded in a single passage around the loop. The loop length is carefully adjusted so the bunches arrive at the linac 180°out of accelerating phase. These bunches then decelerate through the cavity, transferring the bunch energy to the linac RF field. The energy-depleted bunches emerge from the linac and are deflected by a weak dipole magnet to a beam dump. Note that accelerating and decelerating bunches may be interleaved one after the other, since they are at different phases of the RF field, so bunches may emerge at the frequency of the cavity, e.g. ∼1 GHz. A high ring current is achieved by injecting small bunches at this rate.

1.2. Status of x-ray ERL projects

The basic principles of ERL operation were demonstrated in the late 1980s [5] and first applied to a low-energy dedicated machine at the Thomas Jefferson National Accelerator Facility (Jlab) in the last half of the 1990s [6]. The key technological advances that enabled the Jlab machine were improvements in superconducting linacs and in high-duty cycle laser-driven photoinjectors. By 2000, it had become clear that ERL technology was advancing rapidly and offered very attractive possibilities as a hard x-ray source. Cornell University started serious consideration of an x-ray ERL [7] and soon CHESS and the Cornell Laboratory for Elementary Particle Physics (LEPP) entered into a collaboration with Jlab to do a design study [8]. The Cornell/Jlab study concluded that an x-ray ERL was feasible, but would require prototyping in order to fully reap the potential benefits as a superior x-ray source. At present, many sites have announced interest in x-ray ERL development [9], including several sites in the US, as well as in England, Germany, China and Japan. As of 2009, significantly funded hard x-ray ERL R&D is proceeding at Cornell (see [10]) and at KEK in Japan (see [11]).

2. Characteristics of a coherent hard x-ray ERL source

In storage rings, the requirements of long-term electron (or positron) storage dominate the way in which the machine can be built. By contrast, in an ERL SR source, the electron beam simply has to be guided around the ring once, or at most a few times. This removes many constraints on the magnetic lattice and allows greater freedom in tailoring of the machine to the requirements of scientific measurements. As opposed to SASE X-FELs currently under construction, which are inherently low-duty cycle-pulsed sources (i.e. x-rays are on only a very small fraction of the time), an ERL may be operated as a quasi-continuous duty source. Thus, an ERL source can serve the same types of experiments now served by third-generation storage ring sources *while at the same time* offering the superior brightness, coherence and time structure characteristic of a laser-driven, dc photo-cathode source and superconducting accelerator.

As stated above, both Cornell University and the KEK Laboratory in Tsukuba, Japan, are performing research and development on coherent hard x-ray ERL sources. The specifications for machines being developed at the two laboratories are quite similar. Thus only the characteristics of the Cornell design are given below.

Outstanding features of the Cornell ERL include high transverse coherence, small, round source size, short native pulse length and continuous operation at a 1.3 GHz bunch rate. Figure 3 and tables 1 and 2 show target values for a 5 GeV ERL upgrade (figure 2) to the existing Cornell synchrotron facility. Calculations were done with SPECTRA 8.0.10 [12]. The

Table 1. ERL parameters for different modes of operation.

	(A) Hi-flux	(B) Hi-coherence	(C) Small charge, short bunch, Hi-Rep rate	(D)[a] high charge, short bunch, Lo-Rep rate
Energy (GeV)	5	5	5	5
Electron $\Delta E/E$	0.0002	0.0002	0.0026	0.0026
RMS bunch length (fs)	2000	2000	<100[b]	<100[b]
Repetition rate (MHz)	1300	1300	1300	0.1
Bunch charge (pC)	77	19	77[c]	1000
Current (mA)	100	25	100[c]	0.1
Emittance (pm) (horizontal = vertical)	30	8	TBD[cd]	500

[a]Mode D uses larger charge bunches, for more x-rays per pulse, at a sufficiently low rate that these bunches need not be energy recovered. Rather, they are dumped prior to reentry into the first linac.
[b]The higher energy spread in modes C and D allows bunch compression prior to select beamlines, which then receive shortened bunches for fast-pulse studies. Most beamlines precede the bunch compressors and receive native 2 ps bunches.
[c]To be determined by future research. The appropriate compromise between bunch charge and current is limited by wake field effects yet to be evaluated. These, in turn, determine the emittance.
[d]To be determined.

machine is very flexible and can operate in one of four modes: (A) high-flux mode, (B) high-coherence mode, (C) a short-pulse, low-charge mode and (D) a short-pulse, high-charge mode. Table 1 summarizes parameters for these several possible modes of operation. Table 2 lists nominal electron and photon source parameters for the ERL and the brightest high-energy third generation sources (existing and under construction).

Spectral brightness and transverse coherent flux both scale inversely with the product of the transverse emittances, which is why the small emittances of the ERL are so significant. Small emittances also facilitate the production of intense nanobeams: any electromagnetic radiation source is limited by the brightness theorem, which states that the beam area times the beam divergences (i.e. the brightness, for a given wavelength and number of photons in the beam) is at best, constant, no matter what passive optical elements are inserted into the beam. Because of this constraint, nanobeam optics invariably trade beam divergence for focal spot size. The ERL has extraordinary brightness, allowing intense, low-divergence nanobeams.

Small ERL emittances lead to both higher coherence and more intense nanobeams compared to storage ring sources. Sub-micron x-ray beams have been a great success of third-generation SR sources [13]–[17]. However, at storage rings that are limited by source sizes that are much larger horizontally than vertically (table 2), the focused intensity with today's optics is commonly $\sim 10^{12}$ x-rays s^{-1} μm^{-2} (a few are better at producing smaller, 100 nm nanobeams). ERLs are nearly diffraction limited in both directions. With improved x-ray optics, now under development in several laboratories, potential exists at the ERL for 1 nm hard x-ray beams with $\sim 10^{11}$–10^{12} x-rays s^{-1} nm^{-2}.

Table 2. Parameters used to calculate spectral brightness and coherent flux in figures 3 and 4. Values for other sources are good faith estimates based on information posted by the sources on their websites. Nominal values were used where possible to give a fair comparison between existing and projected sources. In the case of NSLS II, the emittances used are for the 8 damping wiggler configuration. All calculations were performed using SPECTRA-8.0.10 [12]. Parameter files are provided in the supplemental information.

	APS	ESRF	Spring8	NSLS II	ERL high coherence	ERL high flux	ERL nanofocus
Electron source							
Energy (GeV)	7.0	6.03	8.0	3.0	5.0	5.0	5.0
$\Delta E/E$ (%)	0.096	0.11	0.11	0.099	0.02	0.02	0.02
Current (mA)	100	200	100	500	25	100	25
ε_N^a (nm · rad)	2.5	4.025	3.4	0.508	0.016[a]	0.06[a]	0.016[a]
Coupling	0.00969	0.006	0.002	0.016	1	1	1
$\varepsilon_x/\varepsilon_y$ (nm · rad)	2.49/0.024	4.0/0.024	3.39/0.007	0.5/0.008	0.008/0.008	0.03/0.03	0.008/0.008
β_x/β_y (m)	14.4/4	0.5/2.73	21.7/14.1	2.02/1.06	3.98/3.98	3.98/3.98	0.16/0.16
α_x/α_y	0/0	0/0	0/0	0/0	0/0	0/0	0/0
η_x/η_y (m)	0.124/0	0.037/0	0.103/0	0/0	0/0	0/0	0/0
η'_x/η'_y	0/0	0/0	0/0	0/0	0/0	0/0	0/0
$\sigma_x/\sigma_y(\mu$m)	224/9.82	60.5/8.10	294/9.78	31.8/2.91	5.64/5.64	10.9/10.9	0.98/0.98
$\sigma'_x/\sigma'_y(\mu$rad)	13.2/2.46	89.5/2.97	12.5/0.69	15.7/2.75	1.42/1.42	2.75/2.75	8.17/8.17
Undulator/x-ray source							
Type	Undulator A	In vacuum undulator	In vacuum undulator	U20 undulator	Helical Delta	Helical Delta	Helical Delta
Beamline	8ID	ID27	BL19XU	Projected	Projected	Projected	Projected
Length (m)	2.4	4	25	3	25	25	0.75
Period (mm)	33	23	32	20	18	18	18
Min. gap (mm)	10.5	6	12	5	5	5	5
$B_{\max}$ (T)	0.891	0.75	0.59	0.97	0.85	0.85	0.85
$K_{\max}$	2.74	1.61	1.76	1.81	1.43	1.43	1.43
$\Sigma_x/\Sigma_y(\mu$m)[b]	224/10.1	60.5/8.56	294.1/12.0	32.1/5.11	8.99/8.99	13.0/13.0	1.55/1.55
$\Sigma'_x/\Sigma'_y(\mu$rad)[b]	14.3/6.21	89.6/5.31	12.6/1.89	18.0/9.21	2.26/2.26	3.26/3.26	13.1/13.1
Spectral brightness[bc]	4.2×10^{19}	1.6×10^{20}	6.4×10^{20}	8.9×10^{20}	8.0×10^{22}	8.9×10^{22}	3.5×10^{21}
Coherent fraction (%)[b]	0.080	0.054	0.085	0.82	24	6.6	36
Coherent flux (ph s^{-1}/0.1%)[b]	2.5×10^{11}	9.5×10^{11}	3.9×10^{12}	5.4×10^{12}	4.8×10^{14}	5.4×10^{14}	2.1×10^{13}

[a]SPECTRA-8.0.10 calculates ε_x and ε_y based on a 'natural emittance' parameter (ε_N) and the coupling constant, so we have included ε_N in this table. Spectra models an isotropic source as having unit coupling, ε_N is therefore double than that of ε_x and ε_y. When comparing an ERL with existing sources, ε_x and ε_y are the relevant parameters, not ε_N.

[b]Values at 8 keV. Σ and Σ' refer to width and divergence, respectively.

[c]Spectral brightness reported in standard units of photons s^{-1} mm^{-2} $mrad^{-2}$/0.1% bw.

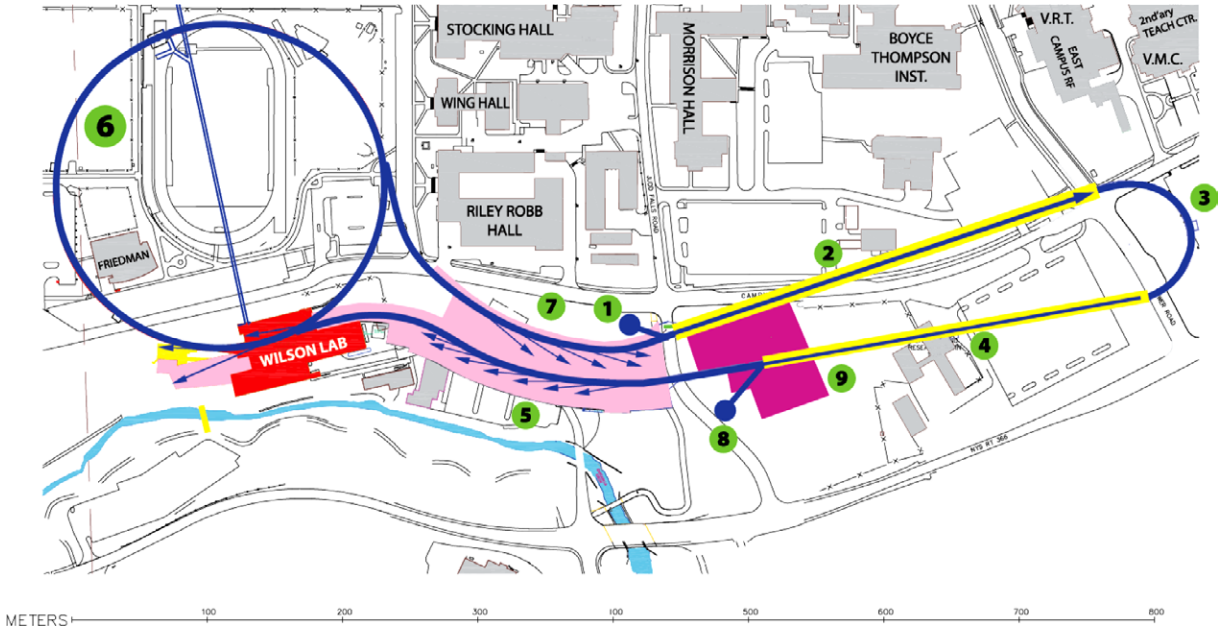

Figure 2. Schematic ERL layout incorporating the existing Cornell Electron Storage Ring (CESR). In modes A–C of table 1, electron bunches are injected (1) and are accelerated to the right in a 2.8 GeV linac (2), loop through a turnaround arc (3) and accelerate to the left through an additional 2.2 GeV linac (4) to 5 GeV. X-ray beamlines are in the pink/red areas. Bunches then pass clockwise around CESR (6) where bunches may be compressed to <100 fs and through more undulators (7) before being uncompressed, energy recovered in a second pass though the linacs (2) and (4), and finally dumped at (8). The ERL concept is extremely flexible. For example, in principle, it would be possible to include an SASE or HGHG X-FEL as part of an ERL facility. In this case, an additional injector would feed large-charge bunches into one of the linacs used by the ERL. These bunches would then be magnetically extracted after the linac and passed though a long undulator for lasing. Studies would be needed to see if an X-FEL can operate simultaneously with other ERL modes.

The one-pass nature of the electron trajectories in the ERL preserves the injector beam properties. The native bunch length from the electron photoinjector, ~ 2 ps, is already much shorter than existing storage ring sources and will be available simultaneously to all x-ray beamlines at an ERL. In addition, magnetic bunch compressors could be used to provide much shorter pulses (<100 fs) at selected stations as noted in table 1.

3. Advantages of an ERL source

The ERL will have very significant advantages for coherent scattering experiments as compared to storage ring sources. X-FEL sources are likely to be complementary with quasi-continuous sources like the ERL. We will outline advantages of the ERL in four categories, and contrast the strengths of the ERL with those of X-FELs.

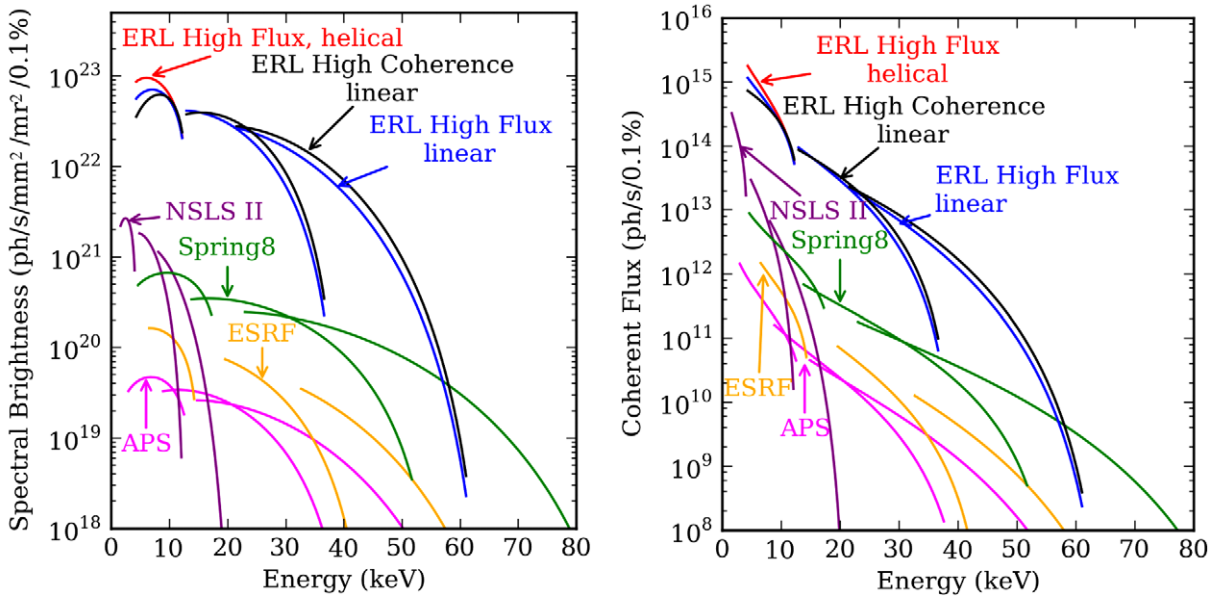

Figure 3. Nominal spectral brightness and coherent flux for various sources, as calculated with SPECTRA using the parameters of table 2. ERL modes (e.g. 'High Flux') are listed in table 1; 'helical' and 'linear' refer to undulator modes described in section 3.3.

3.1. Outstanding coherent flux

The ERL will produce outstanding coherent flux (the number of photons s^{-1} bandwidth $unit^{-1}$ within the solid angle defined by the transverse coherence angles $\lambda/2\pi\,\Sigma_{x,y}$), where λ is the wavelength and Σ is the bunch width, as in table 2; the high coherent fraction as seen in figure 4. In standard units, total coherent flux $F_c = B(\lambda/2)^2$, where B is the spectral brightness. Figure 3 shows, for example at 10 keV, the 25 m ERL Delta undulator (see section 3.3) will produce about 2.4×10^{14} coherent photons $s^{-1}/0.1\%$ bw, about 100 times higher than NSLS-II 3 m ID-U20, and 1500 times that of APS undulator-A (table 2 gives calculation parameters), and will exceed all sources up to 60 keV. This has immediate, profound advantages for coherent scattering and imaging.

Consider, for example, the signal-to-noise ratio for an ergodic process in x-ray photon correlation spectroscopy (XPCS), $S/N = \beta n\eta\sqrt{T\tau}\sqrt{\tau F}\sqrt{P}$, where β, η and τ are the purity of incident coherence, detector efficiency and exposure interval, respectively, and n, T and F are the mean count rate (proportional to incident coherent flux), total measurement time and frame rate $(\tau + \text{exposure readout time})^{-1}$, and P is the number of detector pixels [18]. It follows, if $F \approx \tau^{-1}$ (readout shorter than exposure), that a 100-fold increase in coherent flux allows 10^4 shorter exposures without a reduction in S/N. The range of coherent flux-based science that will be enhanced or enabled by the ERL is compelling. XPCS, used to explore dynamical properties of matter, is currently limited by coherent flux to time scales greater than 1 s at scattering vector length $Q \approx 1\,\text{Å}^{-1}$ and 10 μs at $Q \approx 10^{-3}\,\text{Å}^{-1}$ (a negative power law relates these quantities at the boundary of what is currently accessible [19]). Inelastic x-ray and neutron scattering and proposed X-FEL pulse delay methods will probe length scales below 1 Å, but cannot sense dynamical processes slower than 100 ns. Thus there is an important gap

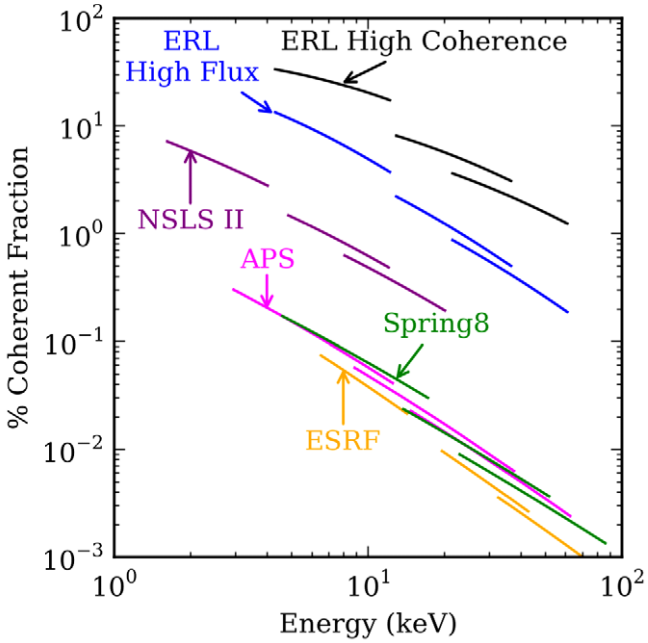

Figure 4. Comparison of nominal coherent fraction (%) for various sources.

(six orders of magnitude in time for $Q \approx 1$ Å^{-1}) that ERL experiments could fill, provided fast area detectors with appropriately sized pixels and fast image readout time become available. Areas ripe for study include systems far from equilibrium, for example, glasses and materials under shear and flow, complex fluids such as polymers and colloidal suspensions, moving domain walls, defects in crystals and protein in solution.

3.2. Round beams

An ERL with near-isotropic transverse emittance will have an approximately round source that is ideal for coherent scattering because the horizontal and vertical transverse coherence lengths will be matched. This means a matched set of optics (or no optics at all) can transport coherent illumination. For example, Fresnel zone plate-based microscopes are most efficient with round beam illumination. At storage rings, transverse coherence lengths typically differ by 10-fold between horizontal and vertical, with the horizontal smaller. On the other hand, area detectors that have revolutionized data collection (note $\sqrt{P}$, above) almost always have square pixels so, for example, XPCS experimenters are faced with difficult choices to match speckle to pixel shape: reduce interference contrast (or incident flux) by opening (closing) horizontal (vertical) slits, or use stronger focusing to match vertical to horizontal coherent spot size.

Each optical element on the beamline (e.g. windows, reflecting surfaces, natural or artificial crystals) must be manufactured to specifications often beyond the state-of-the-art to preserve the wavefront. It is important to minimize and/or simplify beamline design where possible. The ERL has characteristics that enable design simplification including, in some cases, optics-less beamlines. The round source makes it possible to develop very flexible undulators, like the Delta undulator [20], which can operate efficiently in helical mode and intrinsically suppresses the on-axis intensity of unwanted higher harmonics. A 5 GeV ERL light source supports short period undulators with first harmonic radiation in the most widely used range 3–12 keV.

This should be compared to lower-energy (∼3 GeV) rings where, for example, 10 keV radiation is best obtained at the fifth harmonic. In this case, for experiments that use the full undulator harmonic bandwidth ('pink beam') experiments (i.e. many XPCS experiments) both higher and lower harmonics must be suppressed. This requires coherence preserving mirrors (for low pass) and wide bandpass multilayers as high-pass filters. Since undulator power scales as the square of ring energy, this requires severe heat load capabilities on the x-ray optics in high-energy machines. Also, the undulator period cannot be too small if the first harmonic is to cover this spectral range.

3.3. Flexibility

Unlike a storage ring, ERL electron beam transport optics need not be periodic for multi-turn storage and there is no separate injection orbit, so advanced insertion devices like the ERL Delta undulator (with small gap in both horizontal and vertical directions) will offer unique beam properties [20]. In the Delta design, the magnetic field changes at fixed gap by sliding magnet arrays along the beam path, somewhat like the APPLE II undulator. But the Delta has a number of advantages: it can produce helical or planar electron trajectory, and in planar mode the wiggle can be in any plane parallel to the undulator axis. The helical mode will be very important for coherent scattering: the total flux is up to twice that in planar mode, only first harmonic radiation is on-axis, and beam polarization is circular, so Thomson scattering is azimuth independent, even at large scattering angle. Furthermore, since electron beam optics do not need to be periodic at the ERL, the beta function can be optimized for each beamline independently. For example, this allows the electron beam to be tailored to the photon beam from a given undulator, optimizing the spectral brightness [21] on a sector-by-sector basis.

Consider XPCS, where every coherent photon is precious. Not only will a long Delta undulator produce unprecedented coherent flux, but in helical mode it will produce more useful photons because the harmonics and excess heat are suppressed on-axis. As seen in figure 4, a high fraction of the total flux is useful, coherent flux. At 10 keV, for example, within the coherence solid angle, the first harmonic radiation is 15 eV wide, integrated coherent flux is 3.4×10^{14} photons s^{-1}, and coherent beam power is 0.54 W. This implies a coherent power density of $\sim 54\ W\ mm^{-2}$ at 60 m.

An ERL will better realize the full potential of long undulators, due to both the ultra-small emittance in both directions and the small energy spread. The energy width of an undulator harmonic, for example, should be inversely proportional to the number of poles, but is dominated by electron energy spread and emittance at existing sources, especially for long undulators [22]. As a result, the ERL pink beam bandwidth from a 25 m undulator is expected to be 0.15%, 3.9 times smaller than a storage ring undulator of comparable length, and about 10 times smaller than shorter existing undulators. In principle, a mirror or multilayer monochromator will not be required to deliver pink beam, although a deflecting mirror may be required to mitigate Bremsstrahlung background. Smaller bandwidth means longer longitudinal coherence, $\Lambda = \lambda(E/\Delta E)$. A high contrast coherent scattering pattern requires optical path length differences, δ (from points in the sample to the detector), such that $\delta \leqslant \Lambda$. In a transmission geometry, $\delta_W = 2W(Q/k)^2$, where W is the sample thickness and Q is the magnitude of the scattering vector. At fixed Q, the factor of 10 smaller energy spread allows a corresponding increase in W; this can be essential for biological systems where absorption lengths are large, and, therefore, scattering signals are small. When transverse illumination size,

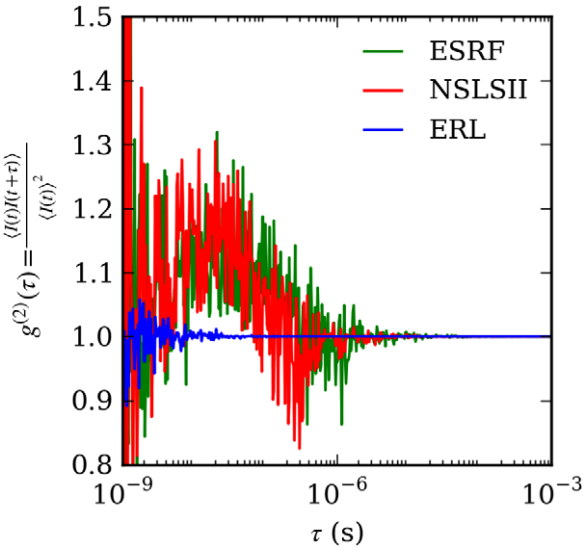

Figure 5. Intensity correlations as a function of delay time τ for different sources. For studies of dynamics at timescales less than 1 μs, the time structure of existing sources (used to mitigate ion trapping) becomes a significant contribution to noise. The ERL is expected to be quasi-continuous down to the 10 ns level.

D, dominates the path length differences, $\delta_D = 2D(Q/k)\sqrt{1-(Q/k)^2}$ (for example with thin, high-Z samples), so large Λ permits a significant increase in obtainable Q. With present day sources, one is often forced to focus (reduce D) and/or reduce bandwidth to achieve acceptable contrast at the required Q. Both alternatives have limitations: the former increases speckle size (for XPCS) relative to pixel size, while the latter reduces flux and signal.

3.4. Quasi-continuous time structure

Because of the short pulse length (2 ps RMS) and high repetition rate (1.3 GHz), the ERL time structure, in modes A and B, will be closer to that of a continuous source than at storage rings. This is very helpful for short exposure time XPCS. One reason is that intensity–intensity correlations, the second-order degree of coherence, $g^{(2)}(\tau) = \langle I(t)I(t+\tau)\rangle / \langle I(t)\rangle^2$, contains much information on temporal correlations in the scattering system. However, the measured $g^{(2)}(\tau)$ is the result of fluctuations in both the sample and 'apparatus', including the source. A short exposure interval samples high-frequency noise on the incident beam, so the most favorable situation occurs when even the shortest exposure averages many x-ray pulses, each of which may have been generated by electron bunches with (hopefully random) charge fluctuations. In practical terms, a 1 μs exposure averages 1300 ERL pulses, while at the APS: in 24-bunch (top-up) mode only 6.4 bunches contribute, and in the most favorable mode 1296-bunch (no top-up) approximately 350 bunches are averaged.

Third-generation sources typically keep some fraction of the electron buckets empty to mitigate ion trapping. Such features in the source time structure present a fundamental challenge for studies of fast dynamics. As seen in figure 5, when the time scale of interest, τ, approaches that of the time structure of the source, the source itself contributes significantly to the value of interest $g^{(2)}$. This problem could possibly be overcome at existing facilities by synchronizing

Table 3. Comparison of beams expected from storage rings, X-FELs and an ERL. All quantities are for $\lambda = 1.5$ Å.

	LCLS@SLAC[a]	X-FEL@DESY[b]	ERL@Cornell[c]
Photons/pulse, N_γ (photons/0.1%)	10^{12}	10^{12}	1.5×10^6
Repetition rate (Hz)	1.2×10^2	4000×10	1.3×10^9
Flux (photons s^{-1}/0.1%)	1.2×10^{14}	3.3×10^{16}	2.0×10^{15}
Flux/beamline (photons s^{-1}/0.1%)	3.0×10^{13} (four beamlines)	3.3×10^{15} (ten beamlines)	2.0×10^{15}
Coherent fraction (%)[d]	74	89	37
Coherent flux (photons s^{-1}/0.1%)	2.2×10^{13}	2.9×10^{15}	4.8×10^{14}
Source size, Σ_r (μm)	33	29.7	9.0
Divergence, Σ'_r (μrad)	0.4	0.4	2.3
Pulse width (ps)	0.02	0.1	2
Spot size at 100 m(μm)	75	72	226

[a][25].
[b][26].
[c]ERL operating in high-coherence mode (see table 1) with 25 m Delta undulator operating in helical mode (see table 2).
[d]The estimated coherent fraction for all three sources is computed from $\lambda^2/[(4\pi)^2 \Sigma_X \Sigma'_X \Sigma_Y \Sigma'_Y]$, where Σ is as defined in table 2.

data acquisition with the source time structure or measuring correlations in the incident beam, adding complexity to an already difficult experiment. The plan for the ERL is to use ion-clearing electrodes to mitigate ion trapping. As a result, the ERL source will be truly quasi-continuous down to nanosecond time scales, which will be important to fill the capability gap between existing XPCS and inelastic scattering techniques.

We do not yet know the degree of bunch-to-bunch charge fluctuations at the ERL. A likely source of noise will be the stability of the lasers used to generate the electrons from the photocathode. A preliminary goal is to limit bunch-to-bunch charge fluctuations to less than 1%.

3.5. Relative merits of the Cornell ERL and current SASE X-FELs for coherence experiments

In this section, for the sake of concreteness, we consider only the relative merits of an ERL as described by tables 1 and 2 and either the European SASE X-FEL being constructed at DESY or the LCLS (see table 3). In addition to these sources, many innovative future light sources are under consideration, including advanced ERLs, ERL-driven X-FELs, x-ray free electron laser oscillators (X-FELOs), seeded free electron lasers, advanced 'ultimate storage ring' designs, etc. However, the performance of such machines is sufficiently speculative that it would be premature to do detailed comparisons.

The nearly diffraction-limited hard ($\lambda < 1.5$ Å) x-ray beams produced by an ERL-driven undulator and the European SASE X-FEL have roughly the same time-averaged spectral brightness per beamline[4] and are nearly ideal for measurements requiring transverse coherence.

[4] Assuming the X-FEL is equally multiplexed across ten beamlines.

The ERL-driven undulator is a quasi-continuous source and the SASE X-FELs are pulsed sources. Conceptually, an ERL-driven undulator will behave very much like a transversely coherent version of a storage ring-driven undulator, but producing orders of magnitude higher coherent flux, which will have immediate applications in coherence-based imaging, time-autocorrelation studies, and crystal-based x-ray optics and spectroscopy. In contrast, the SASE X-FEL produces very intense, ultrashort ($\sim$100 fs or shorter) pulses.

Since the pulse length of the X-FEL is shorter than the typical hundreds of fs phonon time scale in condensed matter, no diffusion of heat from the illuminated volume occurs during the x-ray pulse. Consider an x-ray beam focused to a beam waist of 100 μm. The absorption length in carbon- or water-based matter for 8–10 keV x-rays is approximately 1 mm; therefore, assume that about half the x-rays in a pulse will be absorbed in a column of matter of volume 1 mm long $\times$ (100 μm)^2 in area, i.e. a volume of 10^{-11} m^3. Assume a typical specific heat for the material of 2×10^6 J K-m^{-3}. In the adiabatic limit, about 10^{10} x-rays are sufficient to raise the temperature of the matter column by roughly 1 K. A pulse of 10^{12} x-rays from an X-FEL pulse will result in a temperature rise of $\sim$100 K, which may be tolerated by some samples, but not all. If, however, the x-ray beam is focused to a 1 μm waist, the temperature will instead rise by 10^6 K. This may be ideal for experiments on hot, dense matter or may not be an issue for situations where many identical copies of a sample exist (e.g. gases, liquids or streams of a given molecule or protein) and fresh sample is available for each pulse. However, experiments requiring survival of the sample for times longer than a single shot will not be feasible without attenuating the x-ray beam.

The challenges of using multiple X-FEL pulses can be seen by extending the treatment developed by Stephenson *et al* [23] and Grübel *et al* [19]. In this analysis, the feasibility of coherence-based techniques such as XPCS and diffractive imaging can be assessed for arbitrary sample compositions and x-ray wavelengths by comparing three quantities: N_{max}, the maximum number of photons per pulse before disturbing the sample; N_{min}, the minimum number of photons required for a measurement; and N_{pulse}, the number of photons in a pulse.

For measurements requiring more than one x-ray pulse, one typically would like to avoid heating the sample by more than a few degrees during the measurement. For simplicity, we assume that the illuminated volume is given by $V = L^2\mu^{-1}$, where L^2 is the beam area, μ^{-1} is the absorption length, and that all the energy is converted into heat. Clearly, this overestimates the heating, as some photo- and Auger electrons and some fluorescent x-rays may escape the illuminated volume, but is useful for order of magnitude arguments. Similarly, to a first approximation, the heat capacity per atom is $3k_{\mathrm{B}}$, where k_{B} is the Boltzmann constant. Thus, the relationship between the number of photons per pulse and the temperature jump is given by

$$N_{\mathrm{max}} = \frac{3k_{\mathrm{B}}L^2}{E\sigma_{\mathrm{abs}}}\Delta T_{\mathrm{max}},$$

where E is the photon energy, σ_{abs} is the absorption cross-section per atom and ΔT_{max} is the maximum tolerable temperature rise, independent of sample density or other properties. As shown in the blue curve in figure 6 (reproduced from [19]) for a $T_{\mathrm{max}} = 1$ K, N_{max} is of the order of 10^8 photons pulse^{-1} for $Z > 20$ and $\lambda = 1.5$ Å. N_{max} increases with decreasing wavelength due to the λ^3 dependency on absorption.

The minimum number of photons required is highly dependent on the measurement being performed. The analysis for XPCS has appeared in the literature previously [19, 23] and the

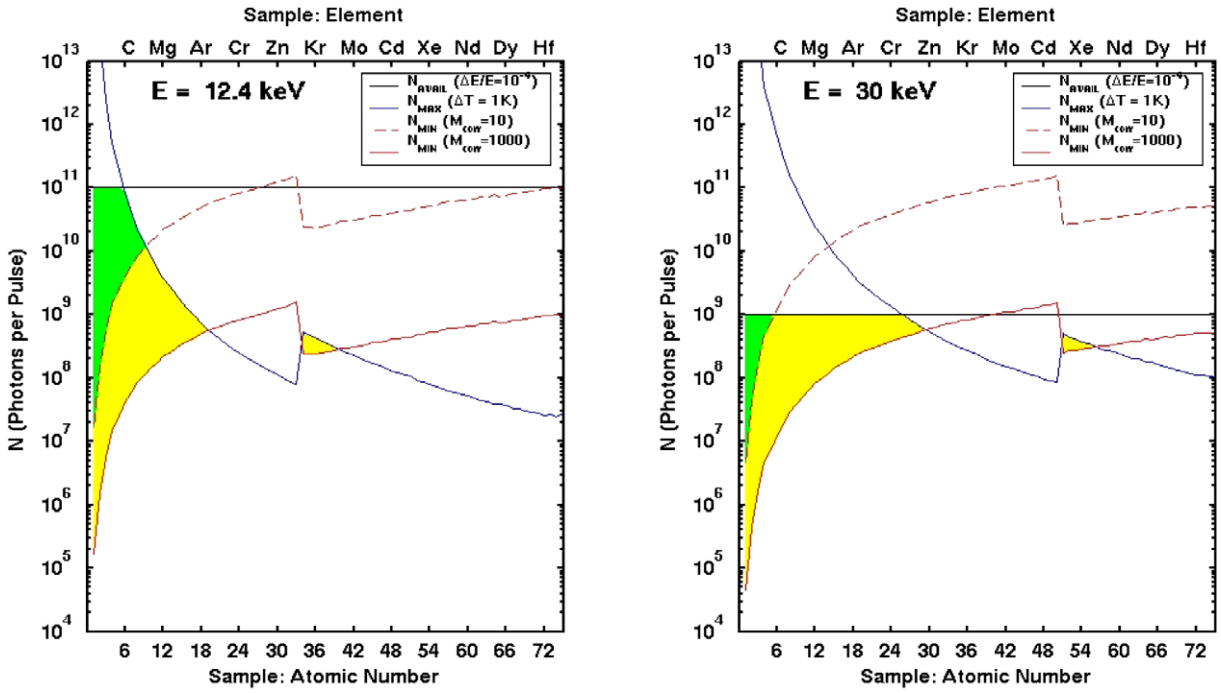

Figure 6. The feasibility of performing XPCS at the LCLS, reproduced with permission from [19]. The blue line indicates the number of incident photons, assuming a sample depth of one absorption length, which heats the sample by 1 K, as a function of atomic number. The red lines indicate the minimum number of photons required to obtain an XPCS dataset, accounting for the number of atoms that scatter coherently, based on $S(Q)$ (10 = dotted line and 1000 atoms = solid line). The solid black line at 10^{11} (left figure) and 10^{9} (right figure) is the number of x-rays per pulse (0.01% bw) produced by the LCLS at 12.4 and 30 keV, respectively. The color-shaded regions indicate the parameter space where conventional XPCS measurements will be possible.

minimum number of incident photons for a measurement is given by

$$N_{\min} = \frac{2\pi L^2 \sigma_{\text{abs}}}{\lambda^2 \sigma_{\text{el}} M_{\text{corr}}} N_{\min}^{\text{SP}},$$

where $N_{\min}^{\text{SP}}$ is the minimum number of photons per speckle and is estimated to be about 10^{-2}, M_{corr} is the number of atoms that scatter coherently, and σ_{el} and σ_{abs} are the total elastic scattering and absorption cross-sections of an atom, respectively. The results of this calculation for a beam area of 100 μm × 100 μm are shown in figure 6, reproduced from Grubel *et al* [19].

The color-shaded regions in figure 6 indicate the parameter space where XPCS measurements will be possible at an X-FEL without beam attenuation. Figure 6 shows that while XPCS will be possible for low atomic number (low Z) materials at an X-FEL, at low x-ray energies it will be necessary to attenuate by beam by up to a factor of 100 to avoid sample heating. In contrast, since the number of photons per pulse at the ERL is comparatively small

and the repetition rate is comparatively high, XPCS will be possible (at least concerning sample heating) for all materials at all energies using the full ERL beam. The implications for XPCS measurements are enormous. In round numbers, the time average flux per beam line for the X-FEL@DESY is roughly the same as for the ERL. Both sources are capable of delivering pulses below 100 fs in duration. However, the ERL delivers x-ray pulses that are about 10^{-6} times less intense, but at a frequency that is roughly 10^6 times as great, thereby mitigating adiabatic heating.

The need to attenuate the beam further exacerbates the difference in time-averaged flux, which directly translates into orders-of-magnitude longer measurement times at the X-FEL. A 1 s XPCS measurement at the ERL will take at least hundreds of seconds on the European X-FEL. (Future X-FELs may be able to achieve higher rates by operating with smaller bunch charges. This is currently under investigation.)

A second promising coherence measurement is diffractive imaging. We can perform a feasibility analysis similar to the XPCS case. Here, we need the coherently scattered intensity at the scattering vector magnitude, Q, appropriate for a spatial resolution of $d = 2R$ for a volume element of radius, R, which is given by Shen *et al* [24] as

$$I(Q = \pi/R) = [1/(4\pi^2)] I_0 N r_0^2 n_0^2 f^2 d^6 \frac{\lambda^2}{2L^2 \cos\theta},$$

where I_0 is the incident flux, r_0 the classical electron radius, n_0 the atom density and $N = V/(\frac{4}{3}\pi R^3)$ is the number of coherent domains in the illuminated volume. For a scattering experiment, higher Z atoms scatter more strongly due to the atomic form-factor, f. Furthermore, if the illuminated volume is once again determined by the absorption length, $V = L^2\mu^{-1}$, more atoms will contribute if there is less absorption. Following Shen *et al* [24], we assume that $I\Delta t = 5$ counts per pixel is a reasonable minimum signal at the highest resolution d producing $I/\sigma_I = 2.24$. Using approximations $f(\pi/R) = Z$ and $\cos\theta = 1$, we obtain

$$N_{\min} = \frac{20\pi^3 L^2 \sigma_{\text{abs}}}{3 r_0^2 \lambda^2 n_0 Z^2 d^3}.$$

To estimate the performance of the ERL, we choose $L = 10\,\mu$m, which keeps the incident flux below the adiabatic heating limit of 1 K for all atomic numbers. Assuming an atom density $n_0 = 10^{22}\,\text{cm}^{-3}$ (typical for condensed matter), $\lambda = 1.5$ Å, $\sigma_{\text{abs}} = 7.6 \times 10^{-27}\,\text{m}^2$, and $Z = 6$ (carbon), we find that such a measurement at $d = 0.5$ nm resolution in principle requires

$$N_{\min} = 2 \times 10^{13} \text{ incident photons.}$$

Figure 7 plots $N_{\min}$ as a function of atomic number, for $\lambda = 1.5$ Å and resolutions $d = 5$, 1.0, 0.25 and 0.1 nm.

In summary, the SASE X-FEL sources will have a dramatic impact on single-shot applications requiring high-peak spectral brightness, such as flash diffraction. The pulse structure of the SASE X-FEL, however, presents a significant challenge for applications of an unattenuated SASE X-FEL as a non- or weakly interacting probe because of the extreme peak intensities. The main point is that neither the ERL nor the X-FEL is appropriate for all types of measurements; the complementary time structures of these two sources will lead to complementary experimental applications.

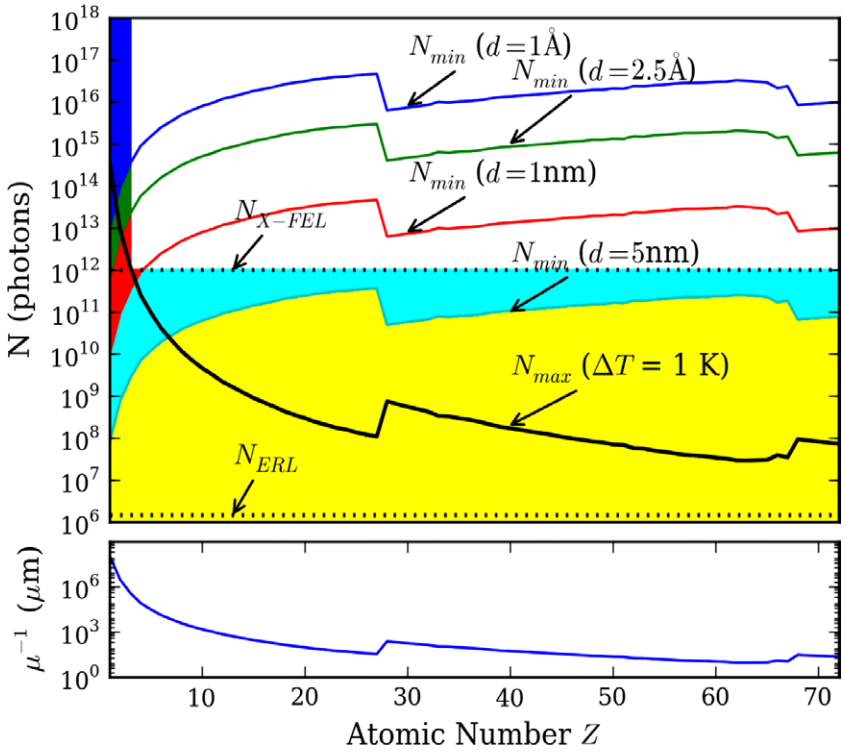

Figure 7. The feasibility of diffractive imaging at an ERL or an SASE X-FEL. Setting the spot size to $(10\,\mu\text{m})^2$ and assuming a sample depth of one absorption length, the minimum number of 1.5 Å photons required to obtain on image with various spatial resolutions is indicated by solid colored curves. Wherever $N_{\text{X-FEL}}$ exceeds N_{max}, the X-FEL exceeds the adiabatic limit and must obtain an image in one pulse. The color-shaded areas map the capabilities of the unattenuated X-FEL, either for single pulse (below the 10^{12} line) or multiple shots ($N_{\text{max}} > 10^{12}$). The unshaded region in the upper-right-hand corner is, in principle, accessible to the ERL or attenuated X-FEL (not accounting for issues like radiation damage). Since each ERL pulse is small, images may be integrated over many pulses to obtain improved signal-to-noise levels.

4. Coherent x-ray science with an ERL

A number of examples of science facilitated by an ERL are given below. Some of these relate most directly to the ability of an ERL source to provide intense nanobeams of x-rays. There is a very close connection in the qualities that optimize an x-ray source for speckle diffraction with coherent x-rays and the qualities that optimize nanofocusing experiments. The common qualities of importance for both applications are the combination of a very small emitting source size along with very high spectral brightness (x-rays $\text{s}^{-1}/0.1\%$ bw $\text{mm}^{-2}\,\text{mr}^{-2}$).

Speckle diffraction requires a sufficiently coherent incident beam in order to achieve the necessary contrast [27]. The transverse coherence requirements are met by limiting the angular size of the beam with an aperture, and the longitudinal coherence by limiting the bandwidth with a monochromator. The resulting coherent intensity is directly proportional to the spectral

brightness of the source. The x-ray source sizes must therefore be small enough that x-rays passing through a pinhole are no more than π out of phase from the different regions of the emitting source. High coherent flux is needed in order to obtain rapid time-resolution data (typically from microseconds to seconds) of the sample under study.

Nanofocusing optics such as Fresnel zone plates [28] and Laue lenses [29] similarly depend on having coherent illumination. Full coherence of the x-ray beam is required across the width of the optic in order to achieve the diffraction-limited small beam size. For a zone plate, for example, this means that the scattering from the outer zone on one side of the zone plate must be in proper phase relationship with scattering from the opposite side in order to make a diffraction-limited nanometer-sized beam. In this sense, every nanobeam x-ray experiment is a coherence-driven experiment whether it explicitly uses the coherence of the x-ray beam or not, as one cannot make the smallest nanobeams without using coherent x-rays from the x-ray source. Since flux through a small aperture (pinhole for speckle or a small area aperture of acceptance in the case of x-ray optics) is proportional to the spectral brightness times the area subtended by the aperture/optic, sources of ultrahigh brightness are required to have enough x-rays in a nanofocused spot so that experiments can be performed in a reasonable length of time.

The high transversely coherent flux, short pulses, and small source size of a 5 GeV ERL will enable a broad range of studies that potentially would lead to paradigm shifts, resolve long-standing questions, and initiate new fields of investigation in coherent x-ray science. The several orders of magnitude increase in average coherent flux over present day sources will be of immediate benefit to a large and established SR community. Enhanced transverse coherence is critical for XPCS and three-dimensional (3D) coherent diffraction imaging. High average brightness at short pulse length and high repetition rate will enable unique studies of molecular dynamics using pump and probe diffraction and orientation-sensitive x-ray spectroscopy. Exceedingly small x-ray source size and divergence is essential for high-pressure research, materials characterization at sub-micron length scales, and small-angle x-ray scattering (SAXS) and WAXS studies of macromolecule dynamics carried on within micro-fluidic flow cells. The opportunity to fully utilize spectral brightness from a 25 m undulator is unprecedented for applications that demand exceedingly high-energy resolution (e.g. inelastic x-ray scattering). The ultra-small beam phase space volume could enable revolutionary new sources like the X-FELO [30]. What follows is a sampling of experiments especially well suited to an ERL source.

4.1. What goes on deep inside the Earth and planets?

The physics and chemistry of deep earth and planetary materials is one of the most important and least understood areas of science [31, 32]. At 100–500 GPa, chemistry is completely altered because the PV term in the free energy exceeds the energy of many chemical bonds. Solid-state properties change because outer electron orbitals overlap, leading to altered electrical properties; indeed, at high pressure almost half the periodic table is superconducting. The invention of the diamond anvil cell (DAC) [33] has revolutionized high-pressure science, and allowed investigations up to center-of-the-earth pressures of 350 GPa [34]. Often high-pressure samples are only microns in size, the x-ray beam must penetrate millimeters of diamond, and pressurization media, like inert gases, solidify and induce strain in the sample. Sample strains require even smaller probe beams to scan and map strain gradients.

Advantages of an ERL: DAC experiments are severely x-ray probe limited, even at the best existing sources. Today a state-of-the-art beamline (APS 16 ID-D) yields 1×10^{10} photons s^{-1} μm^{-2} [35]. Focused X-FEL nanobeams will be of limited use because the peak intensity will damage diamonds. A focused, monochromatic 30 keV x-ray beam from the fifth harmonic of a 5-m ERL undulator would provide $> 10^{13}$ photons s^{-1} μm^{-2}. This huge gain will enable presently unfeasible DAC studies that will transform HP research.

For example, little is known about high-pressure dynamical processes that determine phase stability, phase transitions, chemical reactivity, diffusivity and transport. Numerous chemical reactions occur as heterogeneous earth-forming materials rise through varying conditions of temperature and pressure during volcanic and tectonic events. These reactions affect earthquakes, volcanism and formation of commercially important mineral deposits. Inside the earth, mixing of chemical species is limited by transport. Because diffusivities vary exponentially with temperature, extrapolating known transport properties to HP is prone to large errors and leaves great uncertainties about deep-earth chemistry. Static measurements that are now made at the APS could be made into dynamic measurements at an ERL.

4.2. Can we improve polycrystalline materials?

Most materials are polycrystalline, and the size, structure and interfaces between crystalline grains often controls material properties. A detailed understanding of polycrystalline materials, and better methods of synthesis, would have far-reaching and profoundly positive effects on society. One of the grand challenges in materials science is to explain the materials properties of polycrystalline substances starting from the measured properties of large perfect crystals. For instance, crack propagation, fatigue and failure in the common metals used for bridges and aircraft parts are of great interest.

What has been lacking is sufficiently detailed, 3D, spatially resolved measurements of deformation and microstructure on length scales of a typical grain. Sub-micron spatial resolution of grains and their interfaces is required to provide definitive benchmarks for theory and simulations. Given such information, scientists could link mesoscopic structure with macroscopic properties to explain strength and failure modes of metals and ceramics, ionic diffusion in fuel cell electrodes, dynamical properties of alloys, etc. As grains shrink, the relative contribution of the surface to the overall free energy becomes increasingly important. This is why nanocrystalline materials often have very different properties than materials of the same composition with micron-sized grains [36]. Nanocrystalline materials have enormous potential for society, but are even harder to analyze at the single crystal level. Hard x-ray beams are among the few probes that can penetrate and measure polycrystalline grain properties within bulk materials on appropriate length scales. It is necessary to non-destructively study crystal morphology, orientation, strain, texture and phase with a spatial resolution below the grain size.

Advantages of an ERL: Of particular interest are microstructural studies of crystal grain size and orientation, local elastic strain and plastic deformation using the differential aperture 3D X-ray microscopy (DAXM) recently developed by the RISØ group at the European Synchrotron Radiation Source (ESRF) [37, 38] and by the ORNL group at the Advanced Photon Source (APS) [39]–[41]. In DAXM, an x-ray beam focused to sub-micron size by a pair of crossed Kirkpatrick–Baez mirrors will produce diffraction from crystal grains along the path length in the sample. A series of images collected as a platinum wire edge is scanned across the sample, shadowing the diffraction pattern and therefore allowing identification of a given

Bragg reflection from a diffracting grain at a particular depth. Presently at the APS a single depth scan requires about 30 min and collecting an array of $80 \times 80 \times 80$ voxels takes about 3 h. With the ERL and appropriate detectors, we estimate that a $1000 \times 1000 \times 1000$ voxel map could be generated in a few seconds, thereby enabling *in situ* real time experiments, such as rapid annealing, plastic and elastic deformation, etc [39]. This advance in methodology would have an enormous impact on understanding polycrystalline materials with sub-micron grains.

Complementary information can be obtained through the use of coherent x-ray diffraction imaging (CDI), in which the far-field diffraction pattern (small angle) from a coherently illuminated sample is analyzed to recover the phase of the scattered wavefield. Assuming the structure of the illuminating wavefield is known, this is equivalent to measuring the complex transmission function of the sample. If the sample is a nanocrystal, then each Bragg peak contains a coherent diffraction pattern that can be analyzed to recover a 3D density map of the diffracting crystal, while ignoring neighboring crystals which have different orientations [42]. Bragg coherent diffractive imaging is extremely sensitive to strain; hence, a 3D diffraction pattern about a single Bragg peak can be used to recover a 3D map of the strain projected onto that peak [43]. Researchers at the APS have recently demonstrated the collection of CDI patterns around multiple Bragg peaks of the same crystal, permitting the creation of a 3D map of a 3D strain vector. By taking advantage of the strain sensitivity and orientation selection of Bragg CDI, it should be possible to map in three dimensions the strain due to finite size and boundary effects in an individual grain in a polycrystalline sample, with nanometers resolution.

The application of CDI is limited by the coherent flux that can be delivered to the sample. A 3D coherent diffraction pattern with $\sim$20 nm resolution currently takes hours to record at the APS. Given the inverse fourth power relationship between resolution and flux [44], at the proposed ERL a 3D CDI pattern at $\sim$2 nm from a radiation hard material could be recorded in a few hours, or a 20 nm resolution pattern recorded in a few seconds. Also, CDI could be performed at considerably higher x-ray energy, where current beamlines suffer from very short coherence lengths, allowing access to higher order Bragg peaks and permitting the design of experiments using DACs.

4.3. Can we determine macromolecular structure without crystals?

Modern bioscience is heavily dependent on the determination of macromolecular structures, the vast majority of which have been determined by x-ray crystallography. Crystallography has been very successful in determining the structure of soluble proteins. Membrane proteins and large protein or protein–nucleic acid complexes constitute a very significant fraction of cellular proteins. Unfortunately, crystallography has been less successful with such samples owing to the difficulty of obtaining suitable crystals. Structure determination by nuclear magnetic resonance (NMR) is limited to relatively small molecules and requires preparation of relatively large amounts of isotopically labeled material. Coherent small-angle electron diffraction can resolve non-periodic structures with Å resolution, but the threshold for radiation damage limits the resolution to about 10 Å for biological molecules [45].

An efficient method for solving macromolecular structures to atomic resolution without the need for crystals would certainly be one of the most transformational biological developments in decades. For this reason, a prime motivation for the development of X-FELs has been the possibility of determining macromolecular structure from the scattering of individual molecules [46], thereby foregoing the need to grow crystals. The low X-FEL repetition rate, however, will limit the method.

Spence, Chapman and colleagues have suggested an approach to circumvent the threshold for radiation damage by delivering fresh molecules in a stream of evaporating water droplets. Elliptically polarized laser light would be used to orient a stream of individual molecules [47, 48]. Alternatively, structural information may be obtained from a sufficiently large number of randomly oriented molecules, even when the recorded diffraction is very weak [49].

Advantages of an ERL: ERLs can achieve greatly increased time-averaged flux density relative to other sources.[5] Calculations on GroEL, a large protein complex, indicate that an ERL beam would allow a 7 Å resolution structure to be obtained in minutes [48][6], orders of magnitude faster than with alternative sources. The data acquisition time appears to scale as the inverse fourth power of the resolution for this system [48]; therefore ERL sources may be the most practical way to solve many important but difficult-to-crystallize biological structures.

4.4. What is the physics of the glass transition?

The 125th anniversary issue of *Science* magazine identified the glass transition as one of the most important outstanding questions in all of science. Likewise, Philip Anderson has said that 'The deepest and most interesting unsolved problem in solid state theory is probably the nature of glass and the glass transition' [50]. How can it be that a liquid, subject to only short-ranged forces, becomes locked into just one of many possible configurations? Many theoretical and computational models have been offered, but detailed structural information is needed to compare competing approaches with realistic atomic assemblies. It has long been recognized that what is needed are better measurements of correlation functions of materials undergoing the glass transition. Ideally, one would like to determine the 3D position of every atom in a volume of glass prepared under different conditions, i.e. the specific atomic structure of the glass. Since glass lacks translational order, crystallographic methods cannot be used to determine the specific atomic structure of a glass particle.

Advantages of an ERL: This information may be obtainable with an ERL. The highly coherent, high average flux capabilities of the ERL provide two independent and complementary approaches to study the glass transition: one approach is to use lensless reconstruction procedures [51, 52] to determine the 3D positions of all atoms in a nanoparticle of glass, such as a metallic glass. The ability to study the atomic structure of amorphous materials would be a true breakthrough for materials sciences and physics. A second approach would measure atomic correlations that give rise to the time-varying speckle patterns analyzed by XPCS [53]. This experiment is ideally suited to the ERL. Factors of 10^2 to 10^3 higher coherent flux enables studies of ergodic processes that probe 10^4 to 10^6 faster time scales, or study with much higher signal-to-noise (linear in coherent flux) for systems under study at existing synchrotrons.

[5] The beam need not be fully coherent, only coherent over the volume of the sample.

[6] For a 25 m undulator at an ERL, the authors assumed an 8 keV flux density of 3×10^{14} photons s^{-1} 0.01% μm^2 scaled to a 10 μm spot. This was based on a previous report [24] that such a flux density could be achieved with 30 : 1 demagnification. However, it is not clear from that previous report that such a flux density would be achieved by squeezing an entire beam of 0.014% bandpass into a 1 μm spot, and therefore could not be scaled to a 10 μm spot. By operating the ERL in high-flux mode, and accepting 0.3% bandpass (approximately the full-width at half-maximum (FWHM) of the first harmonic of the undulator), it is possible for the ERL to achieve the required 3×10^{16} photons s^{-1} in a 10 μm spot to support this analysis. The restrictions on path length difference at 7 Å resolution with 0.3% bandpass would require the transverse sample size to be less than 120 nm, and the thickness less than 500 nm.

A very recent and exciting demonstration of cross-correlation analysis of the scattering produced by coherent beam illumination has been published [54]. The work shows how a four-point cross-correlation function can be used to explore local symmetries in colloidal glasses. X-ray scattering from a coherently illuminated disordered (glassy state) liquid produces the usual Q-dependent pattern of radial rings (corresponding to length scales). If, however, the time scale of structure change is slow compared to measurement time, each ring is a speckle pattern. Analyzing angular correlations within the ring (comparing speckle intensity versus angle separation around the ring), the authors found hidden azimuthal symmetry (particular n-fold patterns are associated with particular rings). Simulations show this to be consistent with close-packed random ensembles of icosahedral clusters. A specific fascinating result, which the authors call dynamic heterogeneity, was found in a ring at $Q = 0.04\,\mathrm{nm}^{-1}$ that evolves from 6- to 5-fold symmetry without a measurable intermediate. Similar phenomena are found in molecular dynamics simulations when icosahedral clusters reorganize in different orientations as bonds break and form.

This work has the potential to be extended to solution systems where the characteristic time for structural change is microseconds rather than seconds. It would require collecting statistically meaningful images before the speckles are averaged away by temporal change. To accomplish this one needs coherent beams of much higher intensity, short x-ray pulses and new detectors that collect and store images very rapidly or contain on-board electronics to perform the angular correlation following each exposure. An X-FEL is an obvious source for such work. However, an ERL has some interesting advantages based on the high time-averaged flux, because one could study one sample through multiple exposures and, therefore, follow the time evolution during non-equilibrium conditioning/processing. It may be possible, for example, to understand the local order just before crystallization. A $10\,\mu$m aperture was used to get partial coherence at ESRF ID10A and data were collected by averaging 50–100, 0.15–0.4 s images [54]. In order not to smooth out the speckle pattern, the total exposure time, several tens of seconds, was matched to the sample relaxation time. At 8 keV the ERL (hi-coherence mode) will produce radiation with roughly 200 times higher coherent fraction than ESRF (see table 2). The ERL produces a beam with isotropic two-dimensional transverse coherence, so speckle contrast would be of equal quality around the ring. The nominal ERL pulse structure, 2 ps separated by 770 ps, will allow for optimization of exposure by selecting the number of pulses per image. This will enable high precision studies of dynamics (along with spatial and angular correlations) by determining how speckle contrast depends on exposure pulse number.

4.5. Can we understand the dynamics of macromolecules in solution?

Many vitally important processes involve changes of macromolecular structure in solution. Changes in solution pH, solvent or ionic environment cause proteins and nucleic acids to fold and unfold, polymers to collapse or disperse, cell cytoskeletal proteins to assemble or disassemble, multimers to come apart or aggregate, macromolecules to adsorb or desorb from surfaces, motor proteins to change the way they 'walk' along tubulin fibers, etc. Understanding these processes experimentally requires a means for rapidly changing solution conditions and a method to probe the subsequent structural alterations. Conventional x-ray methods are limited to changes on millisecond time scales, and even then are feasible only if adequate quantities of solution are available. These limitations exclude the vast majority of macromolecular systems of interest. The recent invention of the lamellar flow x-ray micromixer [55, 56] allows solution

conditions to be changed on microsecond time scales. These mixers take advantage of the fact that diffusional equilibrium occurs on microsecond time scales for adjacent lamellar flows that are sub-micron in thickness, and require low-volume, micron-wide streams that conserve scarce chemicals. Lamellar micromixers have been applied to understand protein [56, 57] and nucleic acid folding [58, 59] using SAXS.

Advantages of an ERL: Solution SAXS is inherently weak and signal strength is exacerbated by specimen dilution and the very small diffracting volumes inside the mixers central lamellar stream. Experimental signal-to-noise is ultimately set by the strength of scatter from the macromolecule solution relative to that from the illuminated side-streams. This necessitates probe beams that are both intense and of sub-micron size to interrogate the central stream with minimal inclusion of side streams. Micromixer experiments are presently limited by source brightness to millisecond or greater time resolution at even the most intense x-ray sources. The extremely intense ERL beams will open a new frontier in studies on protein molecule dynamics not presently accessible, enabling micromixer experiments at microsecond or shorter time scales, studies of more weakly scattering systems, and providing higher spatial resolution.

4.6. Can we better understand interfacial processes and defects?

Interfaces profoundly influence the behavior of electronic devices and chemical reactions. Yet surface defects are extraordinarily hard to visualize and analyze: they are non-periodic and occur at very low areal densities. Most often defects disrupt underlying surface periodicity and have an elemental composition similar (if not equal) to the substrate. In these cases, the defects perturb the electronic structure, but fail to fluoresce at a distinguishable x-ray wavelength. Electron methods (e.g. RHEED, etc) are of limited use with buried interfaces, or if the environment of interest is not compatible with high vacuum such as a reaction chamber.

Advantages of an ERL: A new phase contrast full-field imaging technique called x-ray reflection interface microscopy allows visualization of molecular scale features at interfaces and on crystal surfaces [60]. However, the method is currently limited by available total flux, since the reflected intensity is generally at best 10^{-5} lower than the incident intensity, and the condensing and objective zone-plate optics further reduce the available flux by 10^{-2}. Feasibility experiments at the APS with $\sim 10^{12}$ photons s^{-1} incident flux required an hour to image a sample. With an ERL beam, the spectral brightness and total available flux would be increased by a factor of 10^4, and would reduce the acquisition time to a fraction of a second. Improvements in integration time for single images could enable studies of nucleation and steps movements during *in-situ* growth. With the ERL's high coherent flux, coherence-based contrast mechanisms like ptychography could be explored.

As an example, figure 8(a) shows an atomic force microscope (AFM) image of $\langle 001 \rangle SrTiO_3$ after pulsed-laser-deposition growth of 11.3 layers of $SrTiO_3$ [61]. The Fourier transform of the AFM image, in figure 8(b), illustrates speckle in the diffuse 'Henzler rings' associated with the island structure. Using an incoherent beam with flux of 6×10^{13} photons $mm^{-2}\, s^{-1}$, the experimentally obtained diffuse scattering profile in figure 8(c) corresponds to the intensity in the white rectangle in figure 8(b). The ERL will provide sufficient coherent flux to study dynamics based on the speckle seen in figure 8(b).

Studies of ferromagnetic and ferroelectric domains and dynamics [62] will be greatly enhanced by the ERL's high coherent flux and quasi-continuous time structure. Other real-time studies of interface-based processes can be imagined, such as grain boundary evolution under

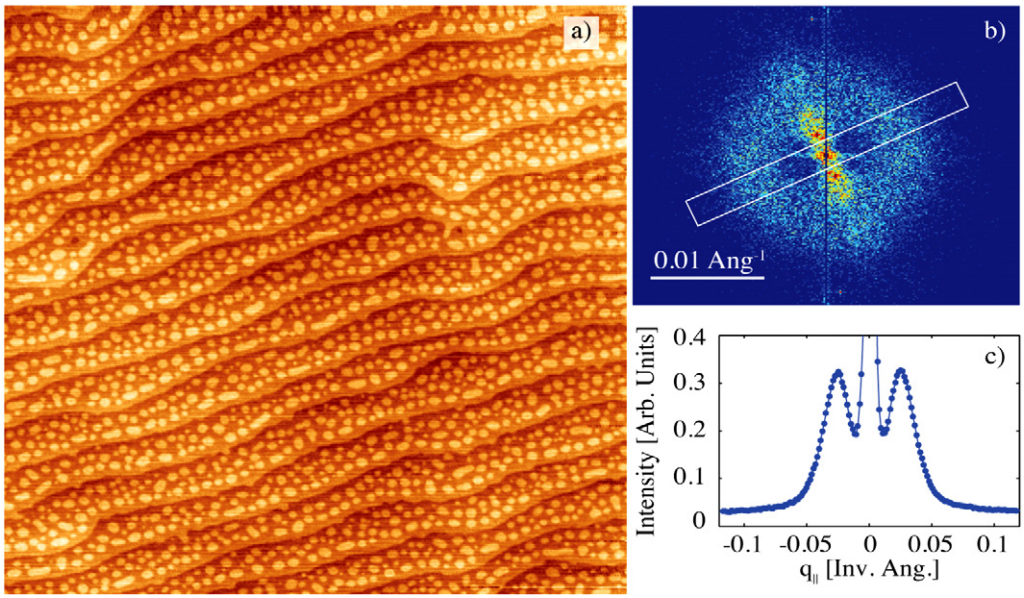

Figure 8. (a) AFM image of $\langle 001 \rangle SrTiO_3$ after pulsed-laser-deposition growth of 11.3 layers of $SrTiO_3$. (b) Fourier transform of the AFM image, illustrating speckle in the diffuse 'Henzler rings' associated with the island structure. (c) Diffuse scattering profile corresponding to the rectangular region in (b), experimentally measured with an incoherent beam.

load. It would be possible to study interfacial reactions under aggressive chemical conditions in reaction vessels, studies that are unfeasible by other methods. Interfacial structural analysis of small-grained materials, such as clays and zeolites, would provide insights into the mechanisms of geochemical reactions important for environmental science. The cumulative impact on surface science will be enormous.

4.7. Can we improve energy storage, photovoltaic and photolytic materials?

Society is in an energy crisis driven by the need to limit carbon emissions, while simultaneously meeting the energy demands of a growing population. Better electrical energy storage is critically needed to match available wind and solar power to load demand, and to make more efficient use of power distribution networks. Hybrid and all-electric vehicles are currently limited by the power and energy density of battery and super-capacitor technologies. Advances in anode, cathode and membrane materials will be required to make fuel cells viable for both mobile and stationary applications. Perhaps the greatest prize of all would be an efficient means of using sunlight to photolyze water into hydrogen and oxygen. Fuel cells, batteries, super-capacitors and photolytic materials depend on complex chemical reactions that result in physical changes, often as a function of charge state. To understand such processes requires probes capable of *in-situ* analysis of electrodes and electrolytes. Frequently, the relevant reactions vary rapidly in time, occur at surfaces and interfaces that are structured at the nanometer level, and are buried deep in nested assemblies. More capable x-ray beams are recognized as necessary to improve and enable energy storage, photovoltaic and fuel cell systems [63]. Improving photovoltaic and photochemical energy conversion systems will require the ability to probe nanometer structures and energy levels at surfaces. Observation of transient effects

that occur on very rapid timescales will also be needed to understand dissipative processes and improve efficiency. Improvements in the efficiency of photovoltaic cells or the capacity of storage batteries and super-capacitors by even a few per cent would have enormous beneficial consequences for society.

Advantages of an ERL: A recent workshop on basic research for electrical energy storage needs [63] made a strong case for sub-micron probes for *in-situ* analysis of catalytic and electrolyte materials in batteries, fuel cells and photovoltaic cells (e.g. Gratzel cells [64, 65]). Understanding these complex materials will require the full arsenal of analytic tools, including advanced x-ray, neutron and electron probes. But even this arsenal has limitations. Progress will require understanding structural changes and chemical reactions on sub-picosecond timescales, in materials that are heterogeneous on sub-micron scales, and buried deep inside active devices. The demands of *in-situ* measurement, often involving solvated environments and need to track over time without destroying the nanostructure precludes many electron microscope and X-FEL methods. Work at an interface and/or at sub-micron size requires intense x-ray nanobeams that peer through solid layers and can be timed to fractions of a picosecond; this limits the feasibility of storage ring sources. In contrast, ERLs are better suited to this work and will be an enabling technology to study materials for energy storage and generation.

5. Summary

The community is actively developing two types of next-generation sources: ERLs and X-FELs. These sources each have quite different properties. As ERLs and X-FELs become available and experience is gained, the community will learn which type of source is optimal for different categories of experiments. ERLs will be especially useful in cases where multiple exposures are required for unique specimens, and where storage ring sources do not provide adequate coherence, nanobeam flux, or sufficiently short x-ray pulses. ERLs are unusually flexible machines, since critical electron beam characteristics are not global functions of the entire ring, as is the case for storage rings operating with equilibrium, stored bunches. The ways in which this flexibility will be used will be revealed with operating experience.

Acknowledgments

The ERL facility described in this paper is the outcome of the labors of well over a hundred people. We gratefully acknowledge the efforts of our ERL colleagues. We thank John Ferguson, Georg Hoffstaetter, Hiroshi Kawata, Florian Loehl, Chris Mayes, Simon Mochrie, Brian Stephenson, Mark Sutton and Maury Tigner for advice on the manuscript. We thank the US National Science Foundation (awards DMR-0225180, DMR-0937466, PHY-0202078 and PHY-0131508) and the State of New York for support. CHESS is also supported, in part by the National Institute of General Medical Science, US National Institutes of Health.

References

[1] DESY 2003 Brilliant future for PETRA III *CERN Courier* **43** 7

[2] Abrikosov I *et al* 2006 *MAX IV Conceptual Design Report* http://www.maxlab.lu.se/maxlab/publications/max4/MAX-IV-CDR.pdf

[3] Ropert A, Filhol J M, Elleaume P, Farvacque L, Hardy L, Jacob J and Weinrich U 2000 Towards the ultimate storage ring-based light source *Proc. EPAC 2000* p 83

[4] Tigner M 1965 A possible apparatus for electron clashing-beam experiments *Nuovo Cimento.* **37** 1228–31
[5] Smith T I, Schwettman H A, Rohatgi R, Lapierre Y and Edighoffer J 1987 Development of the SCA/FEL for use in biomedical and materials science experiments *Nucl. Instrum. Methods Phys. Res.* A **259** 1–7
[6] Neil G R *et al* 2000 Sustained kilowatt lasing in a free-electron laser with same-cell energy recovery *Phys. Rev. Lett.* **84** 662
[7] Gruner S, Bilderback D and Tigner M 2000 Synchrotron radiation sources for the future *Internal Report* (Ithaca, NY: CHESS, Cornell University) http://erl.chess.cornell.edu/papers/WhitePaper_v41.pdf
[8] Gruner S M and Tigner M (ed) 2001 Phase I Energy Recovery Linac (ERL) Synchrotron Light Source at Cornell University *CHESS Technical Memo 01-003; JLAB-ACT-01-04* (Ithaca, NY: Cornell University) http://erl.chess.cornell.edu/papers/2001/ERLPub01_7.pdf
[9] Bisognano J 2009 Future SRF-linac based light sources: initiatives and issues *SRF-2009* http://accelconf.web.cern.ch/AccelConf/srf2009/papers/frobau01pdf
[10] Cornell_ERL 2009 http://erl.chess.cornell.edu/papers/papers.htm
[11] KEK_ERL 2009 http://pfiqst.kek.jp/ERLoffice/index.html
[12] SPECTRA http://radiant.harima.riken.go.jp/spectra/ (cited 18 November 2009)
[13] Riekel C 2000 New avenues in x-ray microbeam experiments *Rep. Prog. Phys.* **63** 233–62
[14] Riekel C, Burghammer M and Muller M 2000 Microbeam small-angle scattering experiments and their combination with microdiffraction *J. Appl. Crystallogr.* **33** 421–3
[15] Riekel C, Burghammer M and Schertler G 2005 Protein crystallography microdiffraction *Curr. Opin. Struct. Biol.* **15** 556–62
[16] Riekel C and Davies R J 2005 Applications of synchrotron radiation micro-focus techniques to the study of polymer and biopolymer fibers *Curr. Opin. Colloid Interface Sci.* **9** 396–403
[17] Roth S V, Burghammer M, Riekel C, Muller-Buschbaum P, Diethert A, Panagiotou P and Walter H 2003 Self-assembled gradient nanoparticle-polymer multilayers investigated by an advanced characterization method: microbeam grazing incidence x-ray scattering *Appl. Phys. Lett.* **82** 1935–7
[18] Falus P, Lurio L B and Mochrie S G J 2006 Optimizing the signal-to-noise ratio for x-ray photon correlation spectroscopy *J. Synchrotron Radiat.* **13** 253–9
[19] Grubel G, Stephenson G B, Gutt C, Sinn H and Tschentscher T 2007 XPCS at the European x-ray free electron laser facility *Nucl. Instrum. Methods Phys. Res.* B **262** 357–67
[20] Temnykh A B 2008 Delta undulator for Cornell energy recovery linac *Phys. Rev. Spec. Top.—Accel. Beams* **11** 120702
[21] Wiedemann H 2003 *Particle Accelerator Physics I: Basic Principles and Linear Beam Dynamics* 2nd edn (Berlin: Springer) pp 325–6
[22] Finkelstein K D, Bazarov I V, Liepe A, Shen Q, Bilderback D, Gruner S and Kazimirov A 2005 Energy recovery LINAC: a next generation source for inelastic x-ray scattering *J. Phys. Chem. Solids* **66** 2310–2
[23] SLAC-R-611 2000 *LCLS The First Experiments* http://www.slac.stanford.edu/pubs/slacreports/slac-r-611.html
[24] Shen Q, Bazarov I and Thibault P 2004 Diffractive imaging of nonperiodic materials with future coherent x-ray sources *J. Synchrotron Radiat.* **11** 432–8
[25] Emma P *et al* 2009 First lasing of the LCLS x-ray FEL at 1.5 Å http://www-ssrl.slac.stanford.edu/lcls/commissioning/documents/th3pbi01
[26] Materlik G and Tschentscher Th (ed) 2001 *TESLA Technical Design Report. Part V. The X-ray Free Electron Laser* http://tesla.desy.de/new_pages/TDR_CD/PartV/xfel.pdf
[27] Sutton M, Mochrie S G J, Greytak T, Nagler S E, Berman L E, Held G A and Stephenson G B 1991 Observation of speckle by diffraction with coherent x-rays *Nature* **352** 608–10
[28] Chao W L, Harteneck B D, Liddle J A, Anderson E H and Attwood D T 2005 Soft x-ray microscopy at a spatial resolution better than 15 nm *Nature* **435** 1210–3
[29] Kang H C, Maser J, Stephenson G B, Liu C, Conley R, Macrander AT and Vogt S 2006 Nanometer linear focusing of hard x rays by a multilayer Laue lens *Phys. Rev. Lett.* **96** 127401

[30] Kim K J, Shvyd'ko Y and Reiche S 2008 A proposal for an x-ray free-electron laser oscillator with an energy-recovery linac *Phys. Rev. Lett.* **100** 244802
[31] Feng J, Grochala W, Jaron T, Hoffmann R, Bergara A and Ashcroft N W 2006 Structures and potential superconductivity in at high pressure: en route to 'metallic hydrogen' *Phys. Rev. Lett.* **96** 017006
[32] Grochala W, Hoffmann R, Feng J and Ashcroft N W 2007 The chemical imagination at work in very tight places *Angew. Chem. Int. Edn Engl.* **46** 3620–42
[33] Jayaraman A 1983 Diamond anvil cell and high-pressure physical investigations *Rev. Mod. Phys.* **55** 65–108
[34] Vohra Y K, Luo H X H and Ruoff A L 1990 Optical-properties of diamond at pressures of the center of earth *Appl. Phys. Lett.* **57** 1007–9
[35] Beamline 16-ID-D 2009 See http://beam.aps.anl.gov/pls/apsweb/beamline_display_pkg.display_beamline?p_beamline_num_c=97
[36] Kumar K S, Swygenhoven H V and Suresh S 2003 Mechanical behavior of nanocrystalline metals and alloys *Acta Mater.* **51** 5743–74
[37] Fu X, Poulsen H F, Schmidt S, Nielsen S F, Lauridsen E M and Jensen D J 2003 Non-destructive mapping of grains in three dimensions *Scr. Mater.* **49** 1093–6
[38] Poulsen H F, Fu X, Knudsen E, Lauridsen E M, Margulies L and Schmidt S 2004 3DXRD—mapping grains and their dynamics in 3 dimensions *Mater. Sci. Forum* **467–470** 1363–72
[39] Ice G E 2006 KB mirrors and nanobeam materials science *ERL Science Workshop* http://erl.chess.cornell.edu/gatherings/erl%20workshop/index.htm
[40] Larson B C, Yang W, Ice G E, Budai J D and Tischler J Z 2002 Three-dimensional x-ray structural microscopy with submicrometre resolution *Nature* **415** 887–90
[41] Yang W, Larson B C, Tischler J Z, Ice G E, Budai J D and Liu W 2004 Differential-aperture x-ray structural microscopy: a submicron-resolution three-dimensional probe of local microstructure and strain *Micron* **35** 431–9
[42] Williams G J, Pfeifer M A, Vartanyants I A and Robinson I K 2003 Three-dimensional imaging of microstructure in Au nanocrystals *Phys. Rev. Lett.* **90** 175501
[43] Pfeifer M A, Williams G J, Vartanyants I A, Harder R and Robinson I K 2006 Three-dimensional mapping of a deformation field inside a nanocrystal *Nature* **442** 63–6
[44] Howells M R *et al* 2009 An assessment of the resolution limitation due to radiation-damage in x-ray diffraction microscopy *J. Electron Spectrosc. Relat. Phenom.* **170** 4–12
[45] Zuo J M, Vartanyants I, Gao M, Zhang R and Nagahara L A 2003 Atomic resolution imaging of a carbon nanotube from diffraction intensities *Science* **300** 1419–21
[46] Neutze R, Wouts R, van der Spoel D, Weckert E and Hajdu J 2000 Potential for biomolecular imaging with femtosecond x-ray pulses *Nature* **406** 752–7
[47] Spence J C H, Schmidt K, Wu J S, Hembree G, Weierstall U, Doak B and Fromme P 2005 Diffraction and imaging from a beam of laser-aligned proteins: resolution limits *Acta Crystallogr.* A **61** 237–45
[48] Starodub D *et al* 2008 Dose, exposure time and resolution in serial x-ray crystallography *J. Synchrotron Radiat.* **15** 62–73
[49] Saldin D K, Shneerson V L, Fung R and Ourmazd A 2009 Structure of isolated biomolecules obtained from ultrashort x-ray pulses: exploiting the symmetry of random orientations *J. Phys.: Condens. Matter* **21** 134014
[50] Anderson P W 1995 Viewpoint: the future (letter) *Science* **267** 1615–6
[51] Miao J W, Ishikawa T, Shen Q and Earnest T 2008 Extending x-ray crystallography to allow the imaging of noncrystalline materials, cells, and single protein complexes *Annu. Rev. Phys. Chem.* **59** 387–410
[52] Rodenburg J M, Hurst A C, Cullis A G, Dobson B R, Pfeiffer F, Bunk O, David C, Jefimovs K and Johnson I 2007 Hard-x-ray lensless imaging of extended objects *Phys. Rev. Lett.* **98** 034801
[53] Sutton M 2002 Coherent x-ray diffraction *Third Generation Hard X-ray Synchrotron Sources: Source Properties, Optics, and Experimental Techniques* ed D M Mills (New York: Wiley) pp 101–23

[54] Wochner P, Gutt C, Autenrieth T, Demmer T, Bugaev V, Ortiz A D, Duri A, Zontone F, Grubel G and Dosch H 2009 X-ray cross correlation analysis uncovers hidden local symmetries in disordered matter *Proc. Natl Acad. Sci. USA* **106** 11511–4

[55] Park H Y, Qiu X Y, Rhoades E, Korlach J, Kwok L W, Zipfel W R, Webb W W and Pollack L 2006 Achieving uniform mixing in a microfluidic device: Hydrodynamic focusing prior to mixing *Anal. Chem.* **78** 4465–73

[56] Pollack L, Tate M W, Darnton N C, Knight J B, Gruner S M, Eaton W A and Austin R H 1999 Compactness of the denatured state of a fast-folding protein measured by submillisecond small-angle x-ray scattering *Proc. Natl Acad. Sci. USA.* **96** 10115–7

[57] Pollack L *et al* 2001 Time-resolved collapse of a folding protein observed with small angle x-ray scattering *Phys. Rev. Lett.* **86** 4962–5

[58] Kwok L W, Shcherbakova I, Lamb J S, Park H Y, Andresen K, Smith H, Brenowitz M and Pollack L 2006 Concordant exploration of the kinetics of RNA folding from global and local perspectives *J. Mol. Biol.* **355** 282–93

[59] Russell R *et al* 2002 Rapid compaction during RNA folding *Proc. Natl Acad. Sci. USA* **99** 4266–71

[60] Fenter P, Park C, Zhang Z and Wang S 2006 Observation of subnanometre-high surface topography with x-ray reflection phase-contrast microscopy *Nat. Phys.* **2** 700–4

[61] Ferguson J, Arikan G, Dals D, Woll A and Brock J 2009 Measurements of surface diffusivity and coarsening during pulsed laser deposition *Phys. Rev. Lett.* **103** 256103

[62] Shpyrko O G *et al* 2007 Direct measurement of antiferromagnetic domain fluctuations *Nature* **447** 68–71

[63] Goodenough J B 2007 Basic research needs for electrical energy storage *Basic Energy Sciences Workshop on Electrical Energy Storage* http://www.sc.doe.gov/bes/reports/files/EES_rpt.pdf

[64] Gratzel M 2003 Dye-sensitized solar cells *J. Photochem. Photobiol.* C **4** 145–53

[65] Gratzel M 2003 Applied physics–solar cells to dye for *Nature* **421** 586–7